DE GRUYTER OPEN

Preparation, characterization of a ceria loaded carbon nanotubes nanocomposites photocatalyst and degradation of azo dye Acid Orange 7

Wen Tao, Tang Yu-bin*, Chen Fang-yan, Mo Bing-yu

Jiangsu University of Science and Technology, China
School of Environmental and Chemical Engineering

*Corresponding author's e-mail: tangyubin@just.edu.cn; ybbill@163.com

Abstract: A ceria loaded carbon nanotubes (CeO_2/CNTs) nanocomposites photocatalyst was prepared by chemical precipitation, and the preparation conditions were optimized using an orthogonal experiment method. HR-TEM, XRD, UV-Vis/DRS, TGA and XPS were used to characterize the photocatalyst. Nitrogen adsorption-desorption was employed to determine the BET specific surface area. The results indicated that the photocatalyst has no obvious impurities. CeO_2 was dispersed on the carbon nanotubes with a good loading effect and high loading efficiency without agglomeration. The catalyst exhibits a strong ability to absorb light in the ultraviolet region and some ability to absorb light in the visible light region. The CeO_2/CNTs nanocomposites photocatalyst was used to degrade azo dye Acid Orange 7 (40 mg/L). The optical decolorization rate was 66.58% after xenon lamp irradiation for 4 h, which is better than that of commercial CeO_2 (43.13%). The results suggested that CeO_2 loading on CNTs not only enhanced the optical decolorization rate but also accelerated the separation of CeO_2/CNTs and water.

Introduction

Ceria (CeO_2) is one of the rare earth oxides that has widely been used in the water gas shift reaction (Rodriguez et al. 2007, Vindigni et al. 2011), automotive three-way catalytic converters (Matsumoto 2004), green phosphors (Long et al. 2006), oxygen storage material (Campbell et al. 2005, Esch et al. 2005), solid fuel cells (Park et al. 2000) and antioxidants in biological model systems (Karakoti et al. 2010, Singh et al. 2011) due to its unique cubic fluorite structure (Trovarelli 2002), oxygen storage capacity (Walton 2011) and high activity.

The photocatalytic oxidation performance of ceria is the focus of research due to its relatively numerous oxygen vacancies and low redox potential (Zhang et al. 2010). Zhai et al. (Zhai et al. 2007) employed homemade CeO_2 nanocrystals as a catalyst for the degradation of 10 mg/L of acid black dye in water in sunlight, and the decolorization rate was 97%. Ji et al. (Ji et al. 2009) and Feng et al. (Feng et al. 2013) used CeO_2 as a photocatalyst to degrade acid orange II, and its photocatalytic ability was better than that of commercial TiO_2 (P25). Because ceria exhibits excellent photocatalytic performance, it is used as a support for loading other catalysts or as the main photocatalyst when it is loaded on other materials. The ability to load nano-sized ceria particles on catalyst supports that have a high specific surface area and stability is required (Guerrero-Ruiz 1994, Soria et al. 1996, Trovarelli et al. 1995).

Because carbon nanotubes have a large specific surface area and specific catalytic property as well as due to the advances in nanotube-walls functionalized research, much interest has been focused on CNTs for use in catalytic chemistry since their discovery in 1991 (Iijima 1991). CNTs exhibit high thermal and chemical stability due to their cylindrical layered, hollow tube nanostructures, which allows them to act as a catalysts to prepare loaded nanometals and metal oxide particles (Peng et al. 2005, Planeix et al. 1994). Researchers from the Chemistry Institute of Chinese Academy of Sciences used CNTs as a support for loading rare earth oxide to prepare CNTs-Eu_2O_3 one-dimensional composite catalysts in 2004 (Fu et al. 2004). Kang et al. (Kang et al. 2005) loaded platinum on CNTs to enhance the structural stability and electronic property of the CNTs. In addition, Rao et al. (Rao et al. 2012) prepared a CeO_2/CNTs composite catalyst to dehydrogenate and oxidize ethylbenzene to styrene in a carbon dioxide atmosphere. Peng et al. (Peng et al. 2005) utilized CeO_2 loaded with CNTs to remove arsenate in water.

However, for the degradation of dye wastewater, researchers only used either CeO_2 as a photocatalyst (Chen et al. 2011, Pouretedal et al .2010) or CNTs as an adsorbent to adsorb pollutants after pretreatment (Gao et al. 2013, Mishra et al. 2010). The use of CeO_2/CNTs nanocomposites materials as photocatalysts for the degradation of azo dyes has not been reported. CeO_2 nanoparticles and CNTs are both suspended in water, which makes their separation from water difficult. The decolorization efficiency of azo dye wastewater using CeO_2 nanoparticles or CNTs is limited. In this paper, we loaded CeO_2 on CNTs to prepare a nanocomposites catalyst that is

easily separated from water and exhibits good decolorization performance to provide a new photocatalyst for the degradation of azo dyes.

Materials and methods

Various reagents employed [commercial CeO_2, $CeCl_3 \cdot 7\,H_2O$, NaOH, polyethylene glycol (PEG 600), ethanol and a concentrated HNO_3 aqueous solution] were purchased from Sinopharm Chemical Reagent Co., Ltd. in 99.99% purity or greater. Multi-walled carbon nanotubes with an average tube diameter of 80 nm and an average tube length of 20 μm were purchased from Nanjing Xianfeng Co., Ltd. Deionized water was used to prepare the solvent and wash sample in this research.

Preparation of nanocomposites photocatalyst
Pretreatment of carbon nanotubes: 1 g of raw CNTs was weighed into a three-necked flask (250 mL capacity), and 100 mL of a concentrated HNO_3 aqueous solution with a volume fraction of 65%~68% was added to the three-necked flask to treat the raw CNTs prior to purification. Then, the mixture was refluxed for 3 h at 125°C. Next, the mixture was successively washed with ethanol at first, then washed with deionized water until pH of 7 was obtained, and afterwards it was cooled to room temperature. Finally, the mixture was placed into a blast oven to dry for 24 h at 60°C and then ground prior to storage.

Preparation of nanocomposites photocatalyst: A known quantity of pretreated carbon nanotubes was mixed with a known quantity of deionized water and then ultrasonically dispersed for 10 min. After adequately stirring for 1 h, a known quantity of $CeCl_3 \cdot 7\,H_2O$ with a mass ratio of Ce to C of 2:3, 1:1, 4:3 or 3:2 and PEG 600 with a ratio of polyethylene glycol mass to the total mass of carbon nanotubes and $CeCl_3 \cdot 7\,H_2O$ of 1% was added. A NaOH aqueous solution (6 g/L) was slowly added dropwise until the pH reached 11.0, 11.5, 12.0 or 12.5, followed by continuous stirring for 1 h, 2 h, 3 h or 4 h, respectively, at room temperature. Then, the mixture was filtered and washed until neutral and dry, which yielded a loose black powder.

Finally, the black powder was dried and placed in a pipe furnace prior to being heated at a heating rate of 5°C/min to 400, 410, 420 or 430°C in air and maintained for 5 min, 10 min, 15 min or 20 min, respectively. Then, the CeO_2/CNTs nanocomposites photocatalyst was obtained.

Characterization of nanocomposites photocatalyst
The morphological features and approximate size of the sample were observed using a Tecnai 12 transmission electron microscope (TEM) made by the Philips Company (Netherlands) and a FEI Tecnai G2 F30 S-Twin 300 KV high-resolution field emission transmission electron microscope (HR-TEM). The crystalline microstructure and phase composition of the sample were evaluated using German Bruker-AXS D8 Advance X-ray diffractometer (XRD), and test conditions were as follows: Cu target, diffuse radiation, tube voltage of 40 kV, tube current of 30 mA, scanning speed of 2 deg/min, scan range 2θ of 20°~80°, and slit width of 0.3 mm. The thermal weight loss of the sample during calcination was determined using an American Perkin Elmer Diamond TGA analyzer in air (TGA) at a heating rate of 5°C/min over a temperature range of 100~700°C. The absorbance threshold of the sample was recorded by a Japanese Shimadzu UV3600 UV-visible spectrophotometer (UV-Vis/DRS) with a scanning wavelength of 200~800 nm. The specific surface area of the sample was calculated using an American Micromeritics ASAP2020 M+C physical adsorption instrument. X-ray photoelectron spectroscopy (XPS) was performed to identify elements and analyze the valence of the elements in the samples using a Japanese ULVAC-PHT PHI 500 VersaProbe X-ray photoelectron spectrometer with a binding energy range of 0~1000 eV.

Photocatalytic degradation experiment
In a typical photocatalytic degradation experiments, 20 mL of Acid Orange 7 aqueous solution of 40 mg/L initial concentration was added to a test tube, then, the pH was adjusted to 5.0. And then, 10 mg of the CeO_2/CNTs nanocomposites photocatalyst was introduced into the test tube and was dispersed by ultrasonic for 5 min. The test tube was then agitated for 1 h in the dark to reach adsorption-desorption equilibrium.

Then, a 500 W xenon lamp was used as the simulated solar light source to irradiate the suspension for 4 h at a distance of 8 cm under uniform stirring. Finally, the absorbance of the supernatant was measured with a visible spectrophotometer at a wavelength of 484 nm to examine the optical decolorizing property of the CeO_2/CNTs nanocomposites photocatalyst after being filtered by a microporous membrane (0.22 μm).

Settling performance experiment
The settling performance of the CeO_2/CNTs, commercial CeO_2 and raw CNTs was tested using an ideal static settling experiment. In a typical settling performance experiment, the suspended particles were evenly dispersed in deionized water and then injected into a settling column. The particles were sampled at the same height, H, of the settling column (starting from the bottom of the settling column, H is 10 cm), at different times, t, followed by measuring the particulate matter concentration, C. Finally, the sedimentation curves were depicted as plots of the concentration ratio, C/C_0 (C_0 represents initial concentration of particulate matter), as a function of the corresponding settling velocity, u (=H/t). Therefore, the total removal of the suspended particles at a known settling velocity was calculated from the plots.

Results and discussion

Results and analysis of the orthogonal test
The stirring reaction time, cerium carbon ratio, pH, calcination temperature and holding time were investigated in this study, and the optical decolorization rate of Acid Orange 7 as evaluation index based on single factor experiments (data not shown) and designed orthogonal test program of five factors and four levels were used to determine the optimum parameters for the preparation of the CeO_2/CNTs nanocomposites photocatalyst. The results and analysis of the orthogonal test for the preparation of CeO_2/CNTs nanocomposites photocatalyst are reported in Tables 1 and 2.

As shown in Table 1, the test results indicated that the highest rate of optical decolorization was observed for No. 11 (62.14%). However, No. 11 may not be the optimal choice. Therefore, further analysis is required.

Level difference analysis was used to investigate the level changes of the various factors that impact the tested items.

When the level difference (R) is larger, there is a greater impact on the factors that vary within a target range for testing indicator values, and the correct factor is the one with the primary influence. The results in Table 2 indicate that the level difference of the calcination temperature is the largest (21.777), which indicated that it has the largest influence on the preparation. Similarly, the level difference for the pH is the smallest (3.947), which indicated that the pH has the smallest effect on the preparation. Therefore, the order of effect of each factor on the photodecolorization rate from largest to smallest is as follows: calcination temperature > holding time > stirring reaction time> cerium carbon ratio > pH.

We determined the theoretical optimal solution (Group A) based on the largest mean value of each factor (i.e., stirring reaction time of 4 h, cerium carbon ratio of 4:3, pH of 11.5, calcination temperature of 410°C and holding time of 5 min).

The choice of the optimal scheme requires a comprehensive analysis and verification test. The preceding analysis indicated that the optimum parameters for the preparation of the CeO$_2$/CNTs nanocomposites photocatalyst include either "No. 11" or Group A. However, the best choice will need to be determined through further testing.

This verification experiment was repeated twice for each of the two schemes mentioned above, and the results indicated that the optical decolorization rates of No. 11 were 62.15% and 61.26%. In addition, the optical decolorization rates for Group A were 66.58% and 68.13%. Obviously, the optical decolorization rates of Group A are still higher than those of No. 11. Therefore, the optimized conditions for the preparation of the CeO$_2$/CNTs nanocomposites photocatalyst are as follows: stirring reaction time of 4 h, cerium carbon ratio of 4:3, pH of 11.5, calcination temperature of 410°C and holding time of 5 min. These conditions are used to prepare the photocatalysts employed in the rest of the experiments.

Characterization of the nanocomposites photocatalyst
TEM/HRTEM
Fig. 1 shows the TEM and HR-TEM images of raw CNTs and the CeO$_2$/CNTs nanocomposites photocatalyst. As shown in Fig. 1a (and inset), the tube-body of the CNTs is clean and well distributed after pretreatment. The TEM images of the CeO$_2$/CNTs nanocomposites photocatalyst are shown in Fig. 1b (and inset), which indicates that the diameter of the CNTs were

**Table 1.** Results from the orthogonal testt

No.	A	B	C	D	E	Photodecolorization rate (%)
1	1	2:3	11.0	400	5	51.73
2	1	1:1	11.5	410	10	52.32
3	1	4:3	12.0	420	15	23.67
4	1	3:2	12.5	430	20	22.41
5	2	2:3	11.5	420	20	24.82
6	2	1:1	11.0	430	15	24.36
7	2	4:3	12.5	400	10	54.13
8	2	3:2	12.0	410	5	57.10
9	3	2:3	12.0	430	10	39.96
10	3	1:1	12.5	420	5	41.82
11	3	4:3	11.0	410	20	62.14
12	3	3:2	11.5	400	15	53.26
13	4	2:3	12.5	410	15	48.85
14	4	1:1	12.0	400	20	54.94
15	4	4:3	11.5	430	5	52.60
16	4	3:2	11.0	420	10	42.99

A: stirring reaction time (h); B: cerium carbon ratio; C: pH; D: calcination temperature (°); E: holding time (min).

Table 2. Analysis of the results from the orthogonal test

Levels	A	B	C	D	E
k_1	37.532	41.340	45.305	53.515	50.813
k_2	40.102	43.360	45.750	55.102	47.350
k_3	49.295	48.135	43.918	33.325	37.535
k_4	49.845	43.940	41.803	34.832	41.078
R	12.313	6.795	3.947	21.777	13.278

A: stirring reaction time (h); B: cerium carbon ratio; C: pH; D: calcination temperature (°); E: holding time (min).
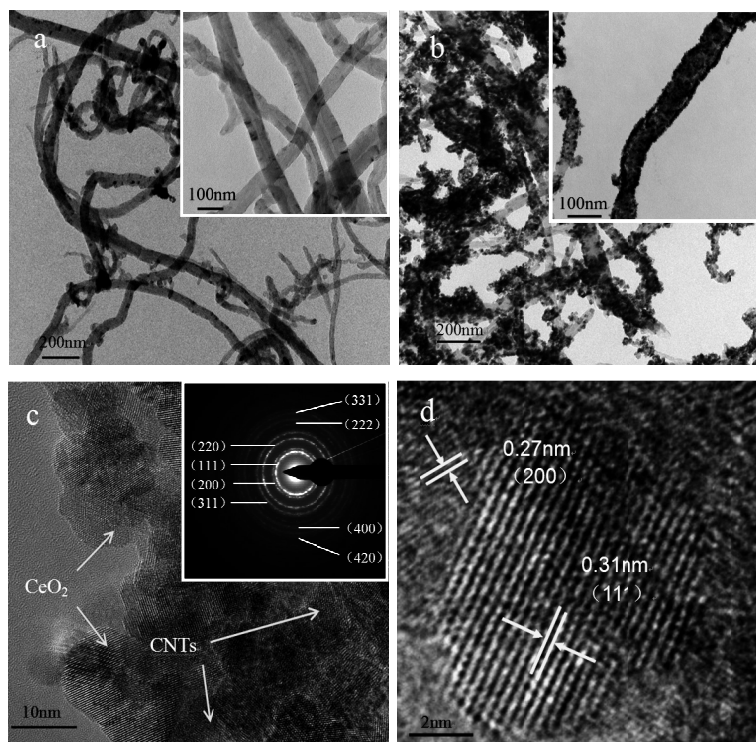
Fig. 1. TEM images of raw CNTs (a), CeO_2/CNTs (b), HRTEM images of CeO_2/CNTs (c&d) and SAED pattern of CeO_2/CNTs (c, inset)

significantly thicker after loading. In addition, the CeO_2 particles are uniformly loaded without agglomeration, which indicates that the product has a high loading efficiency. As shown in the HRTEM images of the CeO_2/CNTs nanocomposites photocatalyst in Fig. 1c, the CeO_2 particles are loaded on the CNTs. In addition, the diameter of the CeO_2 particle is 6 nm~10 nm with a single size distribution, which corresponds to the nanoparticle. The results in Fig. 1c (inset) indicate that the SAED pattern consists of a ring pattern. This typical polycrystalline ring pattern corresponds to the face-centered cubic polycrystalline structure of CeO_2 (Zhang et al. 2007). Fig. 1d shows a single CeO_2 nanoparticle, and the CeO_2 lattice fringes are clearly visible. The observed lattice spacing (i.e., 0.31 nm and 0.27 nm) are in good agreement with the calculated ones for the (111) and (200) crystal planes of the cubic fluorite phase of CeO_2 (Sathish et al. 2011).

XRD

Fig. 2 shows the XRD pattern of the CeO_2/CNTs nanocomposites photocatalyst. As shown in Fig. 2, the main peaks corresponded to the graphene structure of CNTs (002) and the face-centered cubic structure of CeO_2 [(111), (200),(220), (311), (222), (400), (331) and (420)], and no impurity peaks were observed. Therefore, no new substances were generated during the preparation. In addition, all of the main peaks of CeO_2 were consistent with the standard cubic fluorite structure of CeO_2 (PDF 34-0394), indicating that the prepared CeO_2 particles have a polycrystalline face-centered cubic structure and exist as CeO_2 (Chen et al. 2012), which is in agreement with the analysis of the SAED spectra. The CeO_2 particle size calculated using the Scherrer equation (Chen et al. 2011) for the strongest peak (111) was 8.53 nm, which was in good agreement with the results of the particle diameter (6~10 nm) obtained from the analysis of the TEM images.
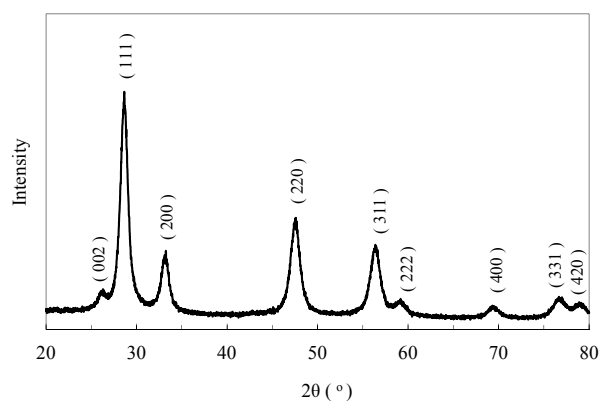
Fig. 2. XRD pattern of the CeO_2/CNTs

TGA

Fig. 3 shows the TG curves of the raw CNTs and the nanocomposites photocatalyst precursor CNTs-Ce $(OH)_3$. The TG curve of the CNTs (grey line) indicated that the CNTs exhibited good heat resistance during calcination, and almost no loss of quality was observed when the temperature was lower than 500°C. When the temperature was higher than 550°C, the weight of the CNTs rapidly decreased, which indicated that the CNTs were being rapidly oxidized. When the temperature reached approximately 580°C, the CNTs completely disappeared. The TG curve of the nanocomposites photocatalyst precursor CNTs-Ce $(OH)_3$ (black line) indicated a weight loss with three steps. The first step occurs at 100~360°C due to the weight loss of precursor dehydration with a mass reduction rate of 3.55%. In the second step from 360°C to 520°C, the precursor weight decreased significantly as the temperature increased, which may be due to dehydrogenation

of the precursor $Ce(OH)_3$ to form CeO_2, and the CNTs were oxidized by the generated CeO_2 with a weight loss rate of 43.45%. When the temperature reached and exceeded 520°C, the sample weight did not vary, which indicated that $Ce(OH)_3$ had been oxidized to CeO_2 and the CNTs had been completely decomposed to water and carbon dioxide.

It should be noted that the heat resistance of the CNTs will be reduced greatly due to the existence of $Ce(OH)_3$ and the generation of CeO_2 in the calcination process, which could reduce the oxidation temperature of CNTs to 360°C. The results of previous single factor impact tests obtained by our group (data not shown) confirmed that CNTs in the precursor would be completely decomposed with a calcination temperature of 430°C and a holding time of 20 min. Therefore, the calcination temperature and holding time of the precursor should not be too high and too long (Zhang et al. 2007). However, the precursor $Ce(OH)_3$ cannot be entirely prevented from converting to CeO_2. In addition, the generated CeO_2 cannot form good crystals when the temperature is too low. Therefore, the calcination temperature should be higher than 400°C (Zhai et al. 2007), which is contradictory for preparing the nanocomposites photocatalyst. Further investigation is required to determine a balance.

At a calcination temperature of 410°C, the weight loss rate of the precursors was 8.39%. After subtracting the water loss rate of 3.55%, the CNT loss rate was less than 5%, which is acceptable during the preparation process. In addition, the calcination temperature of 410°C is reasonable and feasible based on the above analysis of TEM and XRD.

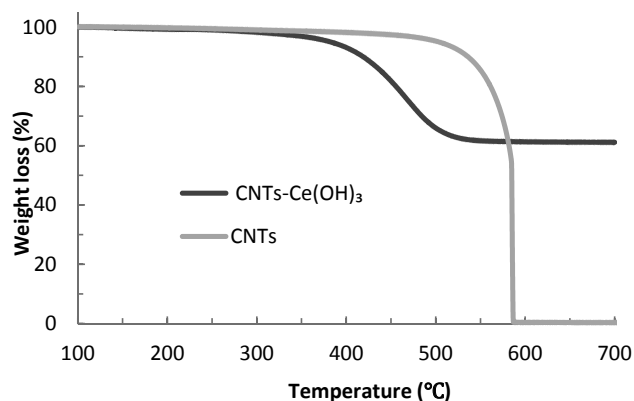**Fig. 3.** TG curve of the CeO_2/CNTs precursor

UV-Vis/ DRS and specific surface area measurements

Fig. 4 shows the UV-Vis diffuse reflectance spectra of the CeO_2/CNTs nanocomposites photocatalyst. As shown in Fig. 4, the prepared nanocomposites photocatalyst exhibited a strong ability to absorb light in the ultraviolet region. In addition, the band gap of the product was observed at approximately 450 nm after making the outside tangent line of the DRS curve. According to the formula $E_g = 1240/\lambda$, the corresponding band gap is 2.76 eV, which is slightly lower than that of 2.81eV, 2.95eV and 3.03eV reported in the literature (Chen et al. 2012, Feng et al. 2013, Zhao et al.2013) and theoretically results in better efficiency of light utilization. The nanocomposites photocatalyst also exhibited some capacity to absorb light in the visible light region, which implies that the utilization of

the xenon lamp simulating solar light to test its photocatalytic property is feasible.

The BET test results of the nanocomposites photocatalyst revealed that the specific surface area of CeO_2/CNTs was 67.82 m²/g, which is nearly 70% higher than the specific surface area of raw CNTs (i.e., 40.00 m²/g) and higher than that of 23.53% reported in the literature (Peng et al.2005). Therefore, an increase in the specific surface area was achieved, resulting in an increased adsorption capacity of the nanocomposites photocatalyst.
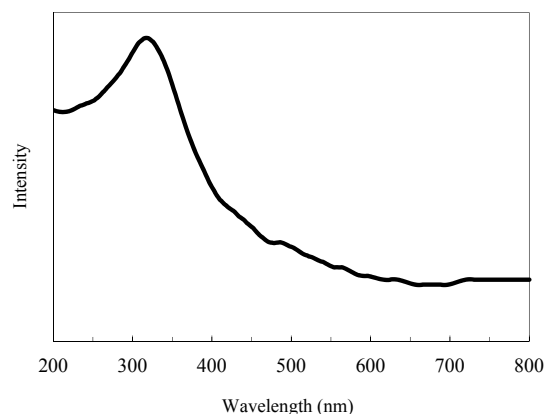

Fig. 4. UV-Vis spectrum of CeO_2/CNTs

XPS

Fig. 5 shows the X-ray photoelectron spectra of the CeO_2/CNTs nanocomposites photocatalyst. The wide spectrum (Fig. 5a) of CeO_2/CNTs only shows the main peaks of the three elements (Ce, O and C) without any other elements, indicating that the sample was not contaminated by other elements during preparation and possesses high purity. Based on the XRD analysis, no incompletely reacted precursors were observed in the product. Fig. 5b shows the XPS Ce 3d spectrum of CeO_2/CNTs. As shown in Fig. 5b, the peaks at 882, 898, 900.5, 907.3 and 916.5 eV can be attributed to Ce (IV), and the peaks at 882 and 898eV correspond to the Ce (IV) $3d^94f^1$ and $3d^94f^0$ final state, respectively. The spin-orbit splitting appears at 900.5, 907.3 and 916.5 eV, which corresponds to 3 u peaks of Ce $(3d)_{3/2}$, indicating that the Ce species in the nanocomposites photocatalyst has a IV valence and exists as CeO_2 (Mei et al. 2010, Park et al. 1996, Zhang et al. 2010). In addition, the O 1s spectrum of the prepared CeO_2/CNTs is shown in Fig. 5c. As shown in Fig. 5c, the O 1s peak is primarily composed of two peaks centered at 529.1 and 531.4 eV, which are due to the lattice oxygen of CeO_2(Rao et al. 2012) and the hydroxyl oxygen on the surface of CNTs or adsorbed oxygen from CeO_2(Lakshminarayanan et al. 2004). In addition, the core level peak, which was located at 529.1 eV, indicated the existence of O^{2-} (Zhang et al. 2007). In addition, the compound has formed a complete CeO_2 lattice structure, which is consistent with the XRD and TEM analysis mentioned above. Therefore, the binding energies of Ce 3d and O 1s detected by XPS are consistent with those of standard CeO_2.

Photocatalytic Performance Testing

The curves for the variation in the Acid Orange 7 concentration during dark adsorption and photocatalytic degradation in the presence of CeO_2/CNTs, commercial CeO_2 and raw CNTs are

shown in Fig. 6a. As shown in Fig. 6a, the rates of Acid Orange 7 adsorption on the three materials in the dark are fast, and the adsorption-desorption equilibrium was achieved in the first 30 minutes. The adsorption efficiency of Acid Orange 7 on the CeO_2 particles without a hole-like or tubular structure was significantly lower than that on CNTs and CeO_2/CNTs. In addition, the total decolorization rate of Acid Orange 7 by the CeO_2/CNTs nanocomposites photocatalyst was as high as 80.58%, and the optical decolorization rate was 66.58% after xenon lamp irradiation for 4 h, which is better than that of commercial CeO_2 (i.e., 43.13%). This result may be due to the adsorption capacity of commercial CeO_2 being lower than that of CeO_2/CNTs, which resulted in the Acid Orange 7 molecules

being more weakly adsorbed on the surface of commercial CeO_2 and affecting its subsequent optical decolorization performance (Chen et al. 2012, Ayanda et al. 2015).

Settling Performance Testing
Fig. 6b shows the sedimentation curves of CeO_2/CNTs, commercial CeO_2 and raw CNTs in water. Based on the integral algorithm (Tang et al.2006), the total removal rate of the CeO_2/ /CNTs suspended particles at a settling velocity of 1.5 cm/min is 59.83%, which is higher than that of CNTs (16.60%) and commercial CeO_2 (44.40%), indicating that the CeO_2/CNTs prepared in this research exhibits good settling performance accelerating its separation from water.
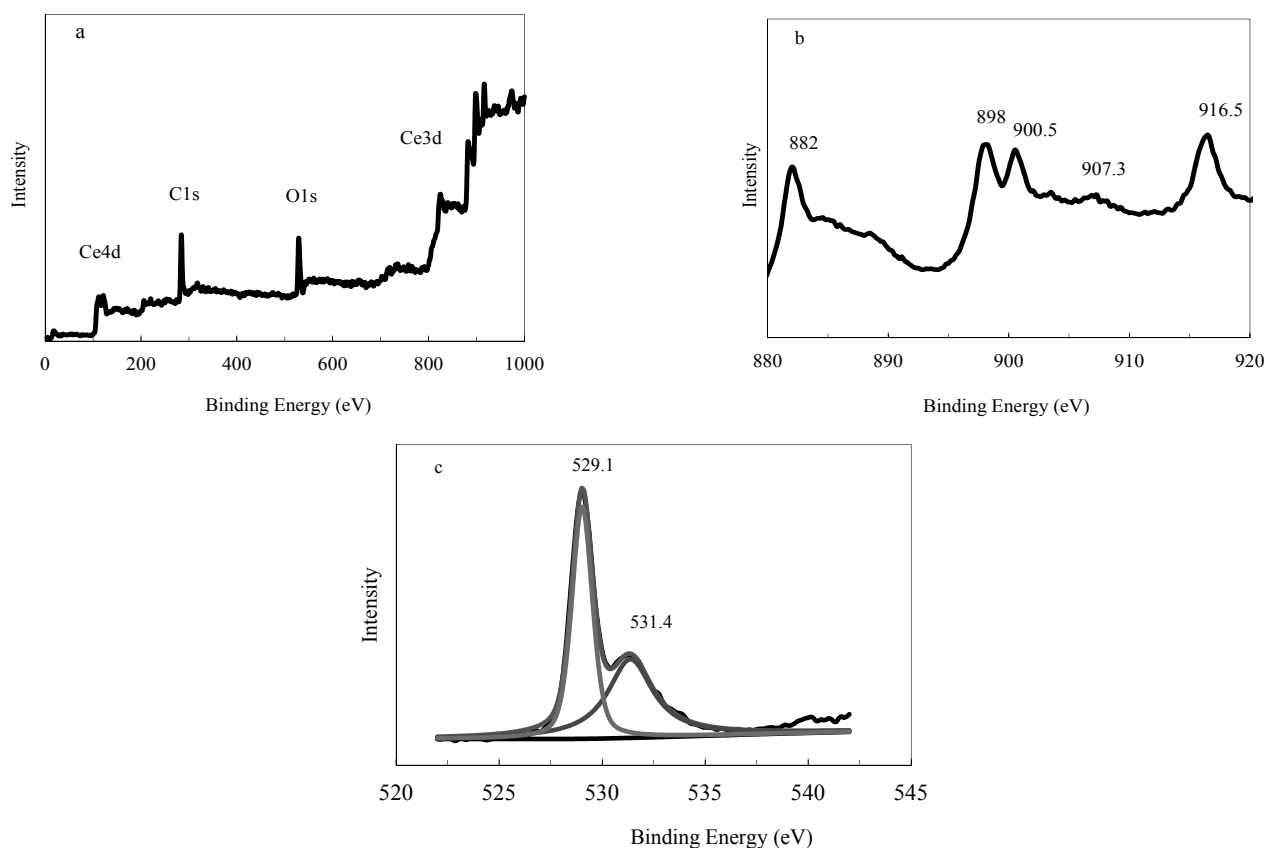

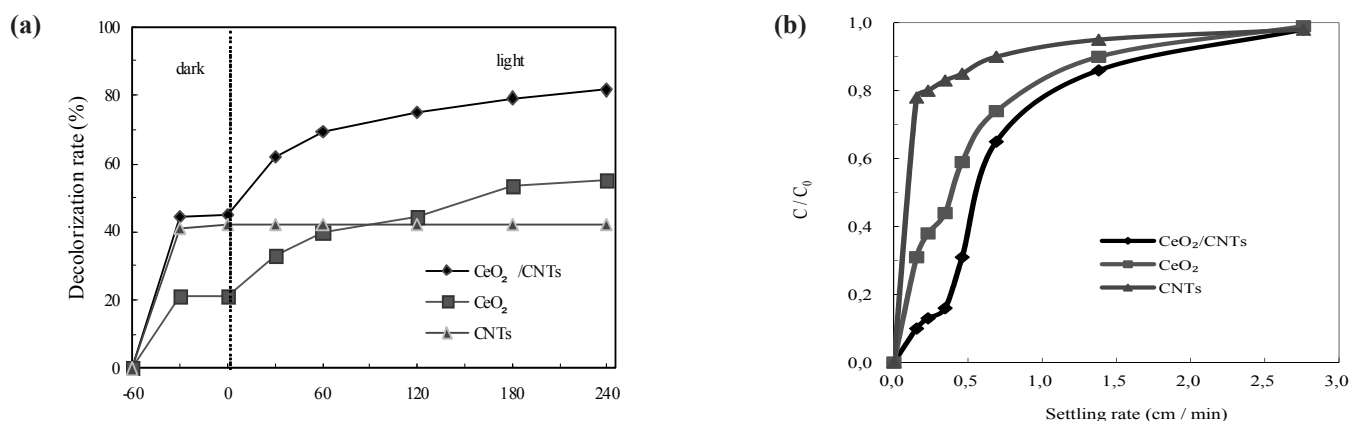Fig. 5. XPS wide spectrum (a), Ce 3d spectrum (b) and O 1s spectrum (c) of CeO_2/CNTs

Fig. 6. Changes in the Acid Orange 7 concentration during dark adsorption and photocatalytic degradation (a) and sedimentation curves (b) in the presence of CeO_2/CNTs, commercial CeO_2 and raw CNTs

Conclusions

CeO_2 can be loaded on CNTs uniformly to prepare a CeO_2/
/CNTs nanocomposites photocatalyst. The optimized conditions
are as follows: stirring reaction time, 4 h; cerium:carbon ratio,
4:3; pH, 11.5; calcination temperature, 410°C; and holding
time, 5 min. The prepared nanocomposites photocatalyst has
no significant impurities, and the size of the CeO_2 loaded on
the CNTs is 6~10 nm. In addition, CeO_2 was dispersed on
the carbon nanotubes with a good loading effect and a high
loading efficiency. The specific surface area of CeO_2/CNTs
is 67.82 m²/g, which is nearly 70% higher than that of raw
CNTs (i.e., 40.00 m²/g), and CeO_2/CNTs exhibits a good
adsorption capacity. In addition, CeO_2/CNTs has a strong
ability to absorb light in the ultraviolet region and exhibits
some capacity to absorb light in the visible light region. The
optical decolorization ratio of CeO_2/CNTs to degrade azo dye
Acid Orange 7 (40 mg/L) was as high as 66.58% after xenon
lamp irradiation for 4 h, which is better than that of commercial
CeO_2 (43.13%) with an improved settling performance. This
result indicates that CeO_2 loaded on CNTs can enhance the
optical decolorization rate and accelerate the separation of
CeO_2/CNTs and water. Therefore, the prepared CeO_2/CNTs
nanocomposites photocatalytic material exhibits potential for
application in the photocatalytic treatment of azo dyes in water.

Acknowledgments

References

Ayanda, O.S., Fatoki, O.S., Adekola, F.A., Ximba, B.J., Akinsoji, O.S. & Petrik, L.F. (2015). Coal fly ash supported nZnO for the sorption of triphenyltin chloride, *Archives of Environmental Protection*, 41, pp. 59-71.

Campbell, C.T. & Peden, C.H.F. (2005). Oxygen vacancies and catalysis on ceria surfaces, *Science*, 309, pp. 713–714.

Chen, F., Shen, X.X., Wang, Y.C. & Zhang, J.L. (2012). CeO_2 & H_2O_2 system catalytic oxidation mechanism study via a kinetics investigation to the degradation of acid orange7, *Appllied Catalysis, B: Environmental*, 121–122, pp. 223–229.

Chen, F., Wang, W., Chen, Z.G. & Wang, T.B. (2012). Biogenic synthesis and catalysis of porous CeO_2 hollow microspheres, *Journal of Rare Earths*, 30, pp. 350–354.

Chen, F.J., Cao, Y.L. & Jia, D.Z. (2011). Preparation and photocatalytic property of CeO_2 lamellar, *Appllied Surface Science*, 257, pp. 9226–9231.

Esch, F., Fabris, S., Zhou, L., Montini, T., Africh, C., Fornasiero, P., Comelli, G. & Rosei, R. (2005). Electron localization determines defect formation on ceria substrates, *Science*, 309, pp. 752–755.

Feng, T., Wang, X.d. & Feng, G.S. (2013). Synthesis of novel CeO_2 microspheres with enhanced solar light photocatalyic properties, *Materials Letters*, 100, pp. 36–39.

Fu, L., Liu, Z.M., Liu, Y.Q., Han, B.X., Wang, J.Q., Hu, P.A., Cao, L.C. & Zhu, D.B. (2004). Coating carbon nanotubes with rare earth oxide multiwalled nanotubes, *Advanced Materials*, 16, pp. 350–352.

Gao, H.J., Zhao, S.Y., Cheng, X.Y., Wang, X.D. & Zheng, L.Q. (2013). Removal of anionic azo dyes from aqueous solution using magnetic polymer multi-wall carbon nanotube nanocomposite as adsorbent, *Chemical Engineering Journal*, 223, pp. 84–90.

Guerrero-Ruiz, A. (1994).Carbon monoxide hydrogenation over carbon supported cobalt or ruthenium catalysts. Promoting effects of magnesium, vanadium and cerium oxides, *Appllied Catalysis, A: General*, 120, pp. 71–83.

Iijima, S. (1991). Helical microtubules of graphitic carbon, *Nature*, 354, pp. 56–58.

Ji, P.F., Zhang, J.L., Chen, F. & Anpo, M. (2009). Study of adsorption and degradation of acid orange 7 on the surface of CeO_2 under visible light irradiation, *Applied Catalysis B: Environmental*, 85, pp. 148–154.

Kang, M., Bae, Y.S. & Lee, C.H. (2005). Effect of heat treatment of activated carbon supports on the loading and activity of Pt catalyst, *Carbon*, 43, pp. 1512–1516.

Karakoti, A., Singh, S. & Dowding, J.M. (2010). Redox-active radical scavenging nanomaterials, *Chemical Society Reviews*, 39, pp. 4422–4432.

Lakshminarayanan, P.V., Toghiani, H. & Pittman, Jr, C.U. (2004). Nitric acid oxidation of vapor grown carbon nanofibers, *Carbon*, 42, pp. 2433–2442.

Long, Z. Q., Ren, L., Zhu, Z.W., Cui, D.L., Zhao, N., Li, M.L., Cui, M.S. & Huang, X.W. (2006). Synthesis of $LaPO_4$: Ce, Terbium by Co-Precipitation Method, *Journal of Rare Earths*, 24, pp. 137–140.

Matsumoto, S. (2004). Recent advances in automobile exhaust catalysts, *Catalysis Today*, 90, pp. 183–190.

Mei, Y., Yan, J.P. & Nie, Z.R. (2010). XPS study on the influence of calcination conditions to cerium ion valence, *Spestroscopy and Spectral Analysis*, 30, pp. 270–273. (in Chinese)

Mishra, A.K., Arockiadoss, T. & Ramaprabhu, S. (2010). Study of removal of azo dye by functionalized multi walled carbon nanotubes, *Chemical Engineering Journal*, 162, pp. 1026–1034.

Park, P.W. & Ledford, J.S. (1996). Effect of crystallinity on the photoreduction of cerium oxide: A study of CeO_2 and Ce/Al_2O_3 catalysts, *Langmuir*, 12, pp. 1794–1799.

Park, S., Vohs, J.M. & Gorte, R.J. (2000). Direct oxidation of hydrocarbons in a solid-oxide fuel cell, *Nature*, 404, pp. 265–267.

Peng, X.J., Luan, Z.K., Ding, J., Di, Z.C., Li, Y.H. & Tian, B.H. (2005). Ceria nanoparticles supported on carbon nanotubes for the removal of arsenate from water, *Materials Letters*, 59, pp. 399–403.

Planeix, J.M., Coustel, N., Coq, B., Brotons, V., Kumbhar, P.S., Dutartre, R., Geneste, P., Bernier, P. & Ajayan, P.M. (1994). Application of carbon nanotubes as supports in heterogeneous catalysis, *Journal of the American Chemical Society*, 116, pp. 7935–7936.

Pouretedal, H.R. & Kadkhodaie, A. (2010). Synthetic CeO_2 nanoparticle catalysis of methylene blue photodegradation: kinetics and mechanism, *Chinese Journal of Catalysis*, 31, pp. 1328–1334.

Rao, R., Zhang, Q.Y., Liu, H.D., Yang, H.X., Ling, Q., Yang, M., Zhang, A.M. & Chen, W. (2012). Enhanced catalytic performance of CeO_2 confined inside carbon nanotubes for dehydrogenation of ethylbenzene in the presence of CO_2, *Journal of Molecular Catalysis A: Chemical*, 363–364, pp. 283–290.

Rodriguez, J.A., Ma, S., Liu, P., Hrbek, J., Evans, J. & Pérez, M. (2007). Activity of CeO_x and TiO_x nanoparticles grown on Au (111) in the water-gas shift reaction, *Science*, 318, pp. 1757–1760.

Sathish, M., Miyazawa, K. & Ye, J. (2011). Fullerene nanowhiskers at liquid-liquid interface: A facile template for metal oxide (TiO_2, CeO_2) nanofibers and their photocatalytic activity, *Materials Chemistry and Physics*, 130, pp. 211–217.

Singh, S., Dosani, T., Karakoti, A.S., (2011). A phosphate-dependent shift in redox state of cerium oxide nanoparticles and its effects on catalytic properties, *Biomaterials*, 32, pp. 6745–6753.

Soria, J., Coronado, J.M. & Conesa, J.C. (1996). Spectroscopic study of oxygen adsorption on CeO_2/γ-Al_2O_3 catalyst supports, *Journal of the Chemical Society, Faraday Transactions*, 92, pp. 1619–1626.

Tang, Y.B., Chen, F.Y. & Zhang, Y.F. (2006). *Water Pollution Control Engineering*, Press of Harbin Institute of Technology, Harbin 2006. (in Chinese)

Trovarelli, A. (2002). *Catalysis by Ceria and Related Materials (Catalytic Science Series, vol. 2)*, Imperial College Press, London 2002.

Trovarelli, A., Deleitenburg, C., Dolcetti, G. & Lorca, J.L. (1995). CO_2 methanation under transient and steady-state conditions over Rh/CeO_2 and CeO_2-promoted Rh/SiO_2: The role of surface and bulk ceria, *Journal of Catalysis*, 151, pp. 111–124.

Vindigni, F., Manzoli, M., Damin, A., Tabakova, T. & Zecchina A., (2011). Surface and inner defects in Au/CeO_2 WGS catalysts: Relation between Raman properties, reactivity and morphology, *Chemistry – A European Journal*, 17, pp. 4356–4361.

Walton, R.I. (2011). Solvothermal synthesis of cerium oxides, Progress in *Crystal Growth and Characterization of Materials*, 57, pp. 93–108.

Zhai, Y., Zhang, S. & Pang, H. (2007). Preparation, characterization and photocatalytic activity of CeO_2 nanocrystalline using ammonium bicarbonate as precipitant, *Materials Letters*, 61, pp. 1863–1866.

Zhang, D.S., Fu, H.X., Shi, L.Y., Fang, J.H. & Li, Q. (2007). Carbon nanotube assisted synthesis of CeO_2 nanotubes, *Journal of Solid State Chemistry*, 180, pp. 654–660.

Zhang, D.S., Mai, H.L., Huang, L. & Shi, L.Y. (2010). Pyridine--thermal synthesis and high catalytic activity of $CeO_2/CuO/CNT$ nanocomposites, *Applied Surface Science*, 256, pp. 6795–6800.

Zhao, P.S., Song, J., Zhou, S.S., Zhu, Y., Jing, L. & Guo, Z.Y. (2013). Facile 1, 4-dioxane-assisted solvothermal synthesis, optical and electrochemical properties of CeO_2 microspheres, *Materials Research Bulletin*, 48, pp. 4476–4480.